Published in final edited form as:
Biomaterials. 2008 August ; 29(22): 3228–3236. doi:10.1016/j.biomaterials.2008.04.029.

TISSUE-TO-CELLULAR LEVEL DEFORMATION COUPLING IN CELL-MICROINTEGRATED ELASTOMERIC SCAFFOLDS

John A. Stella[1], **Jun Liao**[1,*], **Yi Hong**[2,3], **W. David Merryman**[1,**], **William R. Wagner**[1,2,3], and **Michael S. Sacks**[1,2]

1*Department of Bioengineering, University of Pittsburgh, Pittsburgh, PA United States*

2*McGowan Institute for Regenerative Medicine, University of Pittsburgh, Pittsburgh, PA United States*

3*Departments of Surgery and Chemical Engineering, University of Pittsburgh, Pittsburgh, PA United States*

Abstract

In engineered tissues we are challenged to reproduce extracellular matrix and cellular deformation coupling that occurs within native tissues, which is a meso-micro scale phenomenon that profoundly affects tissue growth and remodeling. With our ability to electrospin polymer fiber scaffolds while simultaneously electrospraying viable cells, we are provided with a unique platform to investigate cellular deformations within a three dimensional elastomeric fibrous scaffold. Scaffold specimens micro-integrated with vascular smooth muscle cells were subjected to controlled biaxial stretch with 3D cellular deformations and local fiber micro-architecture simultaneously quantified. We demonstrated that the local fiber geometry followed an affine behavior, so that it could be predicted by macro scaffold deformations. However, local cellular deformations depended *non-linearly* on changes in fiber microarchitecture and ceased at large strains where the scaffold fibers completely straightened. Thus, *local* scaffold microstructural changes induced by macro-level applied strain dominated cellular deformations, so that monotonic increases in scaffold strain do not necessitate similar levels of cellular deformation. This result has fundamental implications when attempting to elucidate the events of de-novo tissue development and remodeling in engineered tissues, which are thought to depend substantially on cellular deformations.

INTRODUCTION

Tissue engineering aims to recapitulate native tissue structure, composition, and mechanical function in a controlled and reproducible manner to overcome the limitations of current medical therapies. The successful development of tissue engineered therapies rests in large part on our ability to employ new materials, manufacturing and processing techniques, and control of cellular mechanobiology. These are all predicated on a strong fundamental knowledge of native cellular and scaffold functional coupling. Cells perceive and react to their mechanical environment through adhesion to local substrates as well as cellular deformations induced by the surrounding mechanical environment. These complex interactions likely play a critical role in the mechanotransduction of proteins required for cell viability and proliferation, and have

For correspondence: Michael S. Sacks, Ph.D., 100 Technology Drive, Room 234, University of Pittsburgh, Pittsburgh, PA 15219, Tel: 412-235-5146, Fax: 412-235-5160, email: msacks@pitt.edu.
*Current address: Department of Agricultural and Biological Engineering, Mississippi State University
**Current address: Department of Biomedical Engineering, University of Alabama at Birmingham

direct implications towards the development of engineered tissues. However, contemporary knowledge is lacking as to how externally applied traction forces at the tissue level are transmitted to the cell in both native and engineered tissue systems. This is in part due to technical difficulties with performing studies in native tissues, which can be confounded by complex hierarchical structures, vasculature, and multiple cell types.

In engineered tissues, various technologies [1–4] have been used to construct layered tissues but have limited abilities to control cellular orientation, while other methods have generated 3D pore structures that show promise in modulating cellular function [5,6]. Yet, irrespective of the particular approach, a key issue remains on how scaffold-level structures and deformations translate to cell level deformations. Cellular deformations are known to strongly affect cellular biosynthetic responses in various tissues [7], yet this important aspect remains largely unexplored in the tissue engineering literature. In native tissues, cells and extracellular matrices (ECM) are regularly arranged to form hierarchical architectures that span multiple length scales to form complex three dimensional tissue systems. Clearly, operational scales have evolved to match the natural scales, and one should focus on the appropriate scales most relevant for the problem at hand [8].

For engineered tissue applications, it is our aim to address the relation between deformations that occur at the cellular level and those that occur at the tissue level due to organ-level forces in a synthetic fibrous scaffold densely integrated with cells. Herein, we utilized poly (ester urethane) urea (PEUU) as the elastomeric scaffold material due to its biodegradable and cytocompatible properties [9]. With our ability to incorporate viable cells distributed throughout the scaffold via concurrent electrospraying and electrospinning (ES) of PEUU fiber scaffolds (Fig. 1-a), we are provided a unique platform to investigate the 3D deformation response of cells seeded in a controlled fiber architecture in-situ [9,10]. Moreover, electrospun scaffolds have structural features that span from μm to multi-mm scales, and are thus analogous to native soft tissue structures. We hypothesize that cellular deformations within ES-PEUU scaffolds are likely a complex function of scaffold mechanical properties, architecture, and cellular coupling with the surrounding polymer fibers. Our objective was therefore to quantify cell deformations and relate them to changes in specific scaffold structures in response to externally applied large (finite) tissue-level strains utilizing real-time laser scanning confocal microscopy (LSCM).

METHODS

Specimen fabrication and preparation

For a detailed account of the concurrent electrospraying and electrospinning process, the interested reader is referred to the previous work of Stankus et al.[9–11]. Briefly, the electrospinning process produces continuous fiber scaffolds exhibiting a wide range of mechanical properties while providing a suitable environment for cell proliferation and growth [9,12–16]. Electrospinning involves the deposition of a solubilized polymer across a large voltage gradient onto a collection surface, with the polymer solution delivered via a small capillary tube where the applied electric potential induces a charge accumulation on the surface of the expelled polymer (Fig. 1-a). Once electrostatic forces exceed viscoelastic forces within the polymer solution and surface tension, a fine jet is ejected towards the collection surface while being accompanied by rapid solvent evaporation. The result is a mat of continuous polymer fibers that, depending upon the processing parameters and polymer utilized, can exhibit mechanical behavior very similar to native soft collagenous tissues [15,17].

For the current study, electrospraying of rat VSMCs was accomplished by feeding 1×10^7 cells/ml into a sterilized capillary charged at 7 kV and located 4 cm from the target mandrel (4.7 mm diameter) concurrent with PEUU/1,1,1,3,3,3-hexafluoroisopropanol solution (12 wt%)

deposition from a capillary charged at 12 kV and located 20 cm from the target mandrel (Fig. 1-a). The mandrel was charged at −4 kV and was rotated at 150 rpm while translating 8 cm along the z-axis at 0.15 cm/s. After 30 min of electrospinning and electrospraying, the microintegrated tube was removed from the mandrel and cultured in a spinner flask at a rotation rate of 15 rpm for 24–48 h prior to imaging. With the capability of simultaneously distinguishing living VSMC nuclei stained with DRAQ5 and PEUU fibers below the specimen surface, an inverted Laser Scanning Confocal Microscope (LSCM, Olympus Fluoview 1000) was chosen.

Biaxial stretch device and testing

Biaxial modes of deformation are well known to better approximate physiological deformations of planar anisotropic tissues [18]. Moreover, we were interested how the scaffold fibers stretch under biaxial deformations without the confounding effects of simultaneous fiber rotations [19]. A biaxial stretcher was thus custom designed for use with an inverted laser scanning confocal microscope (LSCM, Olympus Fluoview 1000). The biaxial stretcher consisted of a polycarbonate specimen chamber with two pairs of orthogonally positioned lead screws (Fig. 1-b). Two loops of 5-0 polyester suture of equal length were attached from the lead screws to each side of the specimens with four custom made stainless steel hooks. Subsurface specimen imaging was facilitated by a glass cover slip (Electron Microscopy Sciences Hatfield, PA, USA) mounted to the stretching device spanning a 30 mm diameter opening in the chamber beneath the specimen. This system was capable of applying both strip biaxial and equibiaxial stretch regimes. Strip biaxial stretch refers to a special loading regime wherein the stretch along one axis is increased while the orthogonal axis is constrained such that no deformation occurs. Conversely, equibiaxial deformation is defined as an equal level of stretch in the two orthogonal specimen directions.

Confocal imaging

An inverted Laser Scanning Confocal Microscope (LSCM) was chosen to observe living cells and scaffold in situ, with images taken via a coverslip window below the specimen. Just prior to imaging, specimens measuring 12 mm square were stained with DRAQ5 for 30 minutes, a far red-fluorescing DNA probe for viable cells. DRAQ5 has been demonstrated not to be toxic to cells with nuclear DNA staining being stable up to 4 h [20]. Moreover, DRAQ5 proved to be DNA staining specific in our experiments allowing us to image live cells concurrently with the auto-fluorescing PEUU fibers. Cell nuclear images were taken under CY5 channel and the scaffold was imaged under CY3 channel via polymer autofluorescence. For each strain level, randomly selected regions were imaged at a subsurface depth ranging from approximately 15–75 μm. For three specimens, 25–86 image stacks were obtained with section thicknesses of 0.972 μm – 2.831 μm with image intervals ranging from 0.6 μm – 0.8 μm, producing a net thickness of 17.4 to 68.0 μm. This imaging approach produced good quality representations of both the nuclei and fibers under stretch (Fig. 1-c,d).

Cellular deformations and scaffold stretch protocols

Nuclear aspect ratio (NAR) has been used as a measure of overall cellular deformation in native tissues (see discussion) [21–24]. For example, aortic heart valve tissues are populated with valvular interstitial myofibroblast cells (AVIC) which serve to maintain the valve leaflet extracellular matrix (ECM) [25, 26]. We have shown [22] that AVICs undergo very large deformations with changes in NAR from 1.8 in the unloaded state to 5.0 under full transvalvular pressure, which is likely related to their biosynthetic function (Fig. 2-a). Thus, to quantify the 3D geometry of the living micro-integrated cell nuclei within the scaffolds, complete LSCM image stacks spanning 15–75 μm were obtained for specimens in the reference and deformed configurations (n=3). From the image stacks we reconstructed the complete 3D VSMC nuclear

surface and observed the cell nuclei consistently exhibited a scalene ellipsoidal geometry (Fig. 2-b). Amira (Mercury Computer Systems, Inc., Carlsbad, CA, USA) was used to stack the registered images and segment cell nuclei manually. Next, MATLAB (The MathWorks, Inc., Natick, MA, USA) was employed to perform principle component analysis (PCA) on the segmented cell nuclei. The full 3D nuclear orientation was computed using principle component analysis of the reconstructed nuclear surface by determining the angles of the three principle nuclear directions with respect to the specimen coordinate axes (α, β, and γ respectively (Fig. 2-c). Cell nuclei aspect ratios of 2D images were quantified using the commercial software Sigma Scan Pro (SPSS Inc., Chicago, IL, USA). For each strain state, the NAR for 80 cells were analyzed with data being presented as AVG ± SEM.

As in our previous work with soft tissues [19,27], we utilized equi-biaxial deformation states (i.e. were the specimen is loaded such that the axial strains, ε_{PD} and ε_{XD}, remain equal), to allow extensional strains without fiber rotations. This was accomplished with both the scaffold fibers imaged by LSCM and also by scanning electron microscopy (SEM) to provide additional detail. Next, in order to induce the largest changes in fiber stretch and rotation, as well as cellular deformations, “strip” biaxial strain states were chosen wherein extensional strain is applied in one direction while the strain the other direction is held at zero. Specific deformation levels utilized included the unloaded configuration followed by states of increasing strip biaxial strain ranging from 5% to 102%, and equi-biaxial strain states of 10% to 50% in 10% increments (n=15 total).

TEM cellular imaging

To verify that NAR could be used as an index of cellular deformations using micro-integrated VSMCs, transmission electron microscopy (TEM) was used to compare and quantify the geometries of the VSMC membrane and nucleus. Due to the polymeric nature of the cell integrated scaffolds it was not possible to fix specimens in their deformed states. As a result, it was only possible to image cells in a free floating configuration. Cell-scaffold construct sections were cut parallel to the preferred and cross-preferred fiber directions for imaging. In total, 22 cells were imaged in the preferred direction while 10 were imaged in the cross-preferred direction. The major and minor axis lengths were then measured manually with the image analysis software Sigma Scan Pro (Systat Software, Inc., San Jose, CA USA). NAR and cell membrane aspect ratios of cells in unstrained PEUU scaffolds were not observed to be significantly different in either the PD or XD directions ($p_{PD} = 0.745$ and $p_{XD} = 0.213$).

Scaffold fiber kinematical analysis

Fiber orientation was also quantified from the LSCM images (Fig. 1-c,d) using custom image analysis software in the unstrained and deformed configurations. Methods for this custom image analysis software have been previously presented in detail [17, 28, 29]. Essentially, the software directly produces statistical distributions of fiber orientation probability, $R(\theta)$, from all measured fibers over the range of all possible orientations, $-90° \leq \theta \leq 90°$. Next, to gain a better understanding of how the ES-PEUU fibers deform as a function of macroscopic scaffold strain, we utilized an affine fiber deformation transformation model to evaluate if the ES-PEUU followed this model, as we have done for collagenous scaffolds [19]. In brief, the measured in-plane deformation gradient tensor (**F**) was first computed from four graphite markers adhered to the surface of the specimen (Fig. 1-b). Polar decomposition of **F** was then performed to remove small rigid body rotations that occur in real time using

$$\mathbf{F}=\mathbf{RU}, \tag{1}$$

where **U** and **R** are the right stretch and rotation tensors, respectively [30]. Essentially, eqn. 1 decomposes the net deformation into rigid body rotations and stretch contributions. In the current study we found that rigid body rotations were negligible, so that $\mathbf{F}\approx\mathbf{U}$. Thus, assuming

a homogeneous, affine deformation the rotation of fibers originally at an angle θ state to the angle β in the deformed state is given by [19]

$$\cot(\beta) = \frac{F_{PD}}{F_{XD}} a\tan(\theta) + F_{PD-XD}, \tag{2}$$

where F_{PD}, F_{XD}, and $F_{PD\text{-}XD}$ are the extensional and shear stretches along the preferred and cross-preferred directions, respectively (Fig. 1-b). If the assumption of affine deformation holds, the angular fiber distribution in the deformed state, R(β), can be related to its original angular distribution R(θ) using

$$R(\beta) = R(\theta)\left[\frac{1}{U_{PD}U_{XD}}\left(F_{PD}^2\cos^2\theta + F_{XD}^2\sin^2\theta\right) + \frac{F_{XD}F_{PD-XD}^2}{F_{PD}}\sin^2\theta + F_{PD-XD}\sin(2\theta)\right]. \tag{3}$$

RESULTS

Fiber kinematics

Comparison of both the LSCM and SEM imaging modes demonstrated the LSCM provided comparable levels of detail, and at least sufficient fiber density to obtain accurate orientation information (Fig. 3-a,b). Upon stretch, a substantial increase in fiber local straightening was observed with increased equi-biaxial stretch (Fig. 3-c,d). Interestingly, at high strain levels there was an upper bound of fiber alignment observed, corresponding to a transition from an ensemble of tortuous fibers seen in the non-deformed specimen to a web-like architecture as manifested by a scaffold with straight, interconnected fibers. Thus, ES-PEUU fibers do not completely loose there tortuosity with strain, and appear to be bonded together. Next, fiber orientation distributions indicated that when unloaded, the fiber network returned immediately back to its original orientation (Fig. 4-a), clearly indicating the elastic nature of the scaffold. Moreover, results for the equi-biaxial tests confirmed that no measurable fiber realignment occurred, as what should occur if the fibers follow the affine model (Fig. 4-b).

In further exploration of the changes in fiber orientation in the strip biaxial strain tests, the fiber orientation distribution R(θ) was observed to become more random with increasing strain (Fig. 5-a). This result was consistent with the fiber network deforming orthogonally from its preferred direction. Next, we assessed whether the ES-PEUU fibers deform according to an affine rule (eqn. 1–eqn. 3) in non-equibiaxial strain states. Interestingly, at both low (Fig. 4-b) and high (Fig. 4-c) strain levels the affine rule predicted good agreement with the experimental data. Thus, due to their high inter-connectivity (e.g. Fig. 3) the fibers in an *average sense* deform in accordance to the bulk strain field.

3D cellular deformations and the relation to local fiber kinematics

From the 3D cellular nuclei reconstructions, we noted that for all measured cells (n = 20) the angle γ, which defined the out-of-plane orientation of the nucleus (Fig. 2-c), was 5.92 ± 1.57° in the unloaded configuration. This indicated that the micro-integrated cells were aligned mainly in the plane of the scaffold. Moreover, under increasing strip biaxial deformation the major principle direction rotated in the direction of deformation (Fig. 6), suggesting substantial mobility with strain.

Next, we examined the interrelationship between the micro-integrated cellular deformations and the changes in scaffolds fibrous structure. This was facilitated by simplifying imaging and analysis to use single section imaging sets to allow for multiple states of deformation to be obtained with same specimen while maintaining cellular viability, which did not result in measureable information loss. No dependency was observed in the NAR-strain relationship for changes in the sequence of deformation, indicating that the cellular-scaffold deformations

were largely elastic in nature. We noted in particular that, under strip biaxial stretch, cells micro-integrated into ES-PEUU scaffolds exhibited a rapid increase in NAR until approximately 60% strain (Fig. 7-a). At strain levels higher than 60%, a plateau in NAR was observed (Fig. 7-a). Moreover, this behavior did not depend upon the direction of strip biaxial stretch (PD vs. XD stretch, Fig. 7-a). Interestingly, the cessation in NAR change with strain corresponded closely with complete straightening of the local fibrous structure (Fig. 3). *This result suggested local fiber straightening, as opposed to macro-tissue level deformations, was the dominant mechanism for inducing cellular deformations.* It should be also noted that this behavior is in stark contrast to that observed in the native tissues, wherein the largest changes occurred at higher stress levels (Fig. 7-b).

DISCUSSION

Choice of scaffold in the study of cellular deformations in engineered tissues

Electrospinning produces continuous fiber scaffolds exhibiting a wide range of mechanical properties, while also providing suitable surfaces for cell proliferation and growth [9,12–16]. The electrospinning process produces scaffold sheets of PEUU fibers (0.8 μm in diameter) approximately 300–400 μm thick to approximate the scale and mechanical behavior of native extracellular matrix, including the ability to undergo large deformations and fully recover when unloaded (i.e. nearly elastic behavior). While electrospinning can fabricate scaffolds that possess ECM-like structures, this morphology also results in pore sizes that are generally smaller (<5 μm) and more tortuous than those produced by other scaffold fabrication methods such as salt leaching [31] and thermally induced phase separation [32]. While it may be possible that cells seeded on the surfaces of electrospun matrices can migrate into the interior by displacing or enzymatically degrading individual fibers, an extended culture period and appropriate signals for cell migration into thick construct interiors might also be required. Thus, while electrospinning permits fabrication of biodegradable elastomeric matrices that resemble the scale, architecture, and mechanical behavior of the native ECM [11], achieving high cellular density and infiltration remains challenging.

To overcome this limitation, we utilized a technique to electrospray cells concurrently while electrospinning PEUU (ES-PEUU) in a manner that allows the control of the degree of fiber alignment and mechanical anisotropy [10,17]. This technique represents a reproducible and relatively rapid method to produce elastomeric fiber reinforced cellularized scaffolds which can mimic the biomechanical properties of native tissues [17] while providing an environment conducive to cell viability. The approach used in the current study centered on our ability to simultaneously quantify the cellular deformation and changes in scaffold fiber architecture under biaxial deformation in-situ.

Use of nuclear aspect ratio

In the present study, cell nuclear aspect ratio was chosen as the metric for cellular deformation. It is known that cell morphology profoundly affects a range of cellular functions, and that changes in the cell cytoskeleton lead to altered stress levels imparted on the nucleus, ultimately affecting cell function. For example, Thomas et al. [7] showed that gene expression and protein synthesis of primary osteogenic cells were altered by changing nuclear shape. Specifically, collagen Type I synthesis correlated directly with nuclear shape, where certain values promoted maximum synthesis, supporting the concept of gene expression and protein synthesis based on optimal distortion of the nucleus. Guilak et al. investigated chondrocyte nuclear deformations under compressive loads in articular cartilage in an attempt to explore how cell deformation may be a stimulus to cell metabolic activity [33]. They observed a reduction in chondrocyte volume with compressive loading, linked to mechanical transduction and signaling through mechano-sensitive channels [34]. We have shown that little AVIC deformation occurs with

the large amount of fiber straightening for pressures below ~1 mmHg, followed by substantial increases in AVIC NAR from 4 to 90 mmHg [22] (Fig. 6-b). Taken as a whole, cell responses to tissue level stresses are modulated through complex micromechanical and fiber-compaction effects that occur under physiological stress levels.

Role of fiber micro-mechanics in cell deformations

The cell micro-integrated ES-PEUU scaffolds exhibited micro-fiber morphologies and kinematics that were shown to directly influence local cellular deformations. For instance, in the unstrained configuration the ES-PEUU fibers exhibited a tortuous architecture which transitioned to a web-like network of straight, interconnected fibers at high levels of strain. The deformations of the micro-integrated VSMC were found to be primarily mediated by this phenomenon. The VSMC integrated ES-PEUU constructs underwent fully recoverable large deformations akin to many native tissues. Moreover, while a non-linear relation between the tissue strain and NAR was observed for both the aortic valve and cell integrated ES PEUU (Fig. 7), the underlying micro-mechanical mechanisms were clearly different. Initially, the integrated VSMC's exhibited a rapid increase in NAR as fibers straightened and tortuosity was reduced. Once the PEUU fibers became straightened and the architecture transitioned to an interconnected web like structure, changes in NAR were observed to plateau. In contrast to the compression mediated deformations observed in the AVIC (Fig. 7-b), the microintegrated VSMC deformation was mediated by the local reduction of tortuosity or straightening of the PEUU fibers (Fig. 7-a). Thus, cell-scaffold interactions can be subtle and can bring about significantly different deformation behaviors.

Broader considerations

Despite its early successes, tissue engineering continues to face challenges in repairing or replacing tissues that serve a predominantly biomechanical function. An evolving discipline called "functional tissue engineering" seeks to address the development of load-bearing structures in several ways [35]. In particular, a critical subset of native tissue mechanical properties must be selected and prioritized as design objectives. This subset is important, given that the mechanical properties of the designs are not expected to completely duplicate the properties of the native tissues. Increasing evidence suggests that mechanical stress, as well as other physical factors, may significantly increase the biosynthetic activity of cells in bioartificial matrices. Clearly, the effects of physical factors on cellular activity must be determined in engineered tissues. Knowledge of these signals may shorten the iterations required to replace a tissue successfully and direct cellular activity and phenotype toward a desired end goal. Ultimately, incorporating each of these principles of functional tissue engineering should result in safer and more efficacious repairs and replacements.

Substantial difficulties are imposed in functional tissue engineering since there are multiple length scales with complex architectures, modes of deformation, and biochemical stimuli which work synergistically to determine physiologic responses. It is generally accepted that both chemical and mechanical factors modulate cell biosynthesis when producing extracellular matrix [34,36–38]. Yet, the exact microstructural characteristics of the scaffolds will have a profound influence on cellular function. For example, collagen and fibrin gels are a popular choice in engineered scaffolds [39–43]. Yet, while possessing desirable characteristics such as cyto-compatibility and anisotropic mechanical properties, their tensile properties have not yet achieved that of native tissues. Moreover, native fibrous protein based gels are largely composed of short-range fibers, whereas native connective tissues are primarily composed of long fibers, which can span multi-mm scales and simultaneously facilitate flexibility and high tensile strength.

As an alternative, biodegradable synthetic polymers as scaffolds to support and encourage tissue regeneration have also proven successful. For example, Freed et al. employed non-woven meshes of polyglycolic acid as a scaffold for seeded chondrocytes and successfully showed the ability to regenerate cartilaginous tissues composed of glycosaminoglycans and collagen [44]. As mentioned previously, electrospinning is a versatile process and slight alterations in the manufacturing process enable the production of scaffolds with a wide array of fiber morphologies (i.e. fiber diameter, porosity, packing density, orientation, etc) which directly influence bulk mechanical properties [45,46]. Controlled mechanical anisotropy, for example, is attained by using a rotating collection surface which induces a preferred fiber direction as the rotational speed of the collector increases [17]. This ability is extremely beneficial in mimicking native tissue architecture and has even been shown to approximate the highly nonlinear biaxial mechanical response of collagenous soft tissues, such as the native porcine pulmonary valve leaflet [17].

In light of these studies, the importance of scaffold-cell mechanical coupling becomes readily apparent in the rational design of engineered tissues. Moreover, the unique micromechanics of various scaffolds induce different cell deformation responses, which could correlate to substantial changes in cell proliferation and function. This phenomenon is illustrated by three grey bars placed at intervals of 20% strain which each correspond to unique NAR values. Instead, the change in cell deformation (or NAR)-strain relationship explored here can be used to guide future engineered tissue applications for these integrated ES PEUU scaffolds.

Limitations

It should be noted that we investigated the response cell integrated ES PEUU scaffolds cultured for 48 hours, which contain minimal functional ECM. The forming ECM within the scaffold and its subsequent micromechanical effects will likely have a substantial effect on cellular deformation, and could prove critical in defining the long term behavior of cell function within integrated electrospun scaffolds. In addition, much of the complex interactions between VSMC and polymeric scaffolds remain unknown, including the nature of cellular focal adhesions to the PEUU matrix. It is likely that the nature and extent of adhesion sites between a cell and its surrounding matrix will directly impact manifestations of biosynthetic activity.

Conclusions

It remains a critical goal to understand how organ-level deformations, such as cyclic stretch, bending, and shear [47,48], translate to microstructural deformations and ultimately as cellular mechanical stimuli. A great deal can be learned about the mechanical modulation of functional tissue from ES-PEUU scaffolds, since they capture some aspects of native tissue microstructure and exhibit the ability to endure large deformations while recovering completely. Moreover, these issues become more challenging in the formation of actively contracting tissues, where cellular contraction must be coordinated at higher scales in order to provide large stresses required for organ contraction. The emergence of new materials and processing methods will clearly be required to meet these functional needs.

ACKNOWLEDGMENTS

Funding for this work was provided by NIH R01s HL68816 and HL69368. John Stella was partially supported by the NIH-NHLBI training grant (T32-HL76124) entitled "Cardiovascular Bioengineering Training Program." Additional support for Drs. Jun Liao and W. David Merryman came from American Heart Association Grant-in-Aid (0565346U) and Pre-doctoral Fellowship (0515416U), respectively.

REFERENCES

1. Yang J, Yamato M, Nishida K, Ohki T, Kanzaki M, Sekine H, Shimizu T, Okano T. Cell delivery in regenerative medicine: the cell sheet engineering approach. J Control Release 2006;116:193–203. [PubMed: 16890320]
2. Ito A, Hayashida M, Honda H, Hata K, Kagami H, Ueda M, Kobayashi T. Construction and harvest of multilayered keratinocyte sheets using magnetite nanoparticles and magnetic force. Tissue Eng 2004;10:873–880. [PubMed: 15265305]
3. Shen JY, Chan-Park MB, He B, Zhu AP, Zhu X, Beuerman RW, Yang EB, Chen W, Chan V. Three-dimensional microchannels in biodegradable polymeric films for control orientation and phenotype of vascular smooth muscle cells. Tissue Eng 2006;12:2229–2240. [PubMed: 16968163]
4. Sun T, Norton D, McKean RJ, Haycock JW, Ryan AJ, MacNeil S. Development of a 3D cell culture system for investigating cell interactions with electrospun fibers. Biotechnol Bioeng 2007;97:1318–1328. [PubMed: 17171721]
5. Boland T, Xu T, Damon B, Cui X. Application of inkjet printing to tissue engineering. Biotechnol J 2006;1:910–917. [PubMed: 16941443]
6. Moutos FT, Freed LE, Guilak F. A biomimetic three-dimensional woven composite scaffold for functional tissue engineering of cartilage. Nat Mater 2007;6:162–167. [PubMed: 17237789]
7. Thomas CH, Collier JH, Sfeir CS, Healy KE. Engineering gene expression and protein synthesis by modulation of nuclear shape. Proc Natl Acad Sci U S A 2002;99:1972–1977. [PubMed: 11842191]
8. Stoneham AM, Harding JH. Not too big, not too small: the appropriate scale. Nat Mater 2003;2:77–83. [PubMed: 12612689]
9. Stankus JJ, Guan J, Fujimoto K, Wagner WR. Microintegrating smooth muscle cells into a biodegradable, elastomeric fiber matrix. Biomaterials 2006;27:735–744. [PubMed: 16095685]
10. Stankus JJ, Soletti L, Fujimoto K, Hong Y, Vorp DA, Wagner WR. Fabrication of cell microintegrated blood vessel constructs through electrohydrodynamic atomization. Biomaterials 2007;28:2738–2746. [PubMed: 17337048]
11. Stankus JJ, Guan J, Wagner WR. Fabrication of biodegradable elastomeric scaffolds with sub-micron morphologies. J Biomed Mater Res 2004;70A:603–614.
12. Zhong S, Teo WE, Zhu X, Beuerman RW, Ramakrishna S, Yung LY. An aligned nanofibrous collagen scaffold by electrospinning and its effects on in vitro fibroblast culture. J Biomed Mater Res A 2006;79:456–463. [PubMed: 16752400]
13. Yoshimoto H, Shin YM, Terai H, Vacanti JP. A biodegradable nanofiber scaffold by electrospinning and its potential for bone tissue engineering. Biomaterials 2003;24:2077–2082. [PubMed: 12628828]
14. Tian F, Hosseinkhani H, Hosseinkhani M, Khademhosseini A, Yokoyama Y, Estrada GG, Kobayashi H. Quantitative analysis of cell adhesion on aligned micro- and nanofibers. J Biomed Mater Res A. 2007
15. Nerurkar NL, Elliott DM, Mauck RL. Mechanics of oriented electrospun nanofibrous scaffolds for annulus fibrosus tissue engineering. J Orthop Res 2007;25:1018–1028. [PubMed: 17457824]
16. Li WJ, Mauck RL, Cooper JA, Yuan X, Tuan RS. Engineering controllable anisotropy in electrospun biodegradable nanofibrous scaffolds for musculoskeletal tissue engineering. J Biomech 2007;40:1686–1693. [PubMed: 17056048]
17. Courtney T, Sacks MS, Stankus J, Guan J, Wagner WR. Design and analysis of tissue engineering scaffolds that mimic soft tissue mechanical anisotropy. Biomaterials 2006;27:3631–3638. [PubMed: 16545867]
18. Sacks MS. Biaxial mechanical evaluation of planar biological materials. Journal of Elasticity 2000;61:199–246.
19. Gilbert TW, Sacks MS, Grashow JS, Woo SL, Badylak SF, Chancellor MB. Fiber kinematics of small intestinal submucosa under biaxial and uniaxial stretch. J Biomech Eng 2006;128:890–898. [PubMed: 17154691]
20. Martin RM, Leonhardt H, Cardoso MC. DNA labeling in living cells. Cytometry A 2005;67:45–52. [PubMed: 16082711]
21. Screen HR, Lee DA, Bader DL, Shelton JC. Development of a technique to determine strains in tendons using the cell nuclei. Biorheology 2003;40:361–368. [PubMed: 12454427]

22. Huang HY, Liao J, Sacks MS. In-situ deformation of the aortic valve interstitial cell nucleus under diastolic loading. J Biomech Eng 2007;129:880. [PubMed: 18067392]
23. Guilak F, Ratcliffe A, Mow VC. Chondrocyte deformation and local tissue strain in articular cartilage: a confocal microscopy study.PG - 410-21. J Orthop Res 1995:13. [PubMed: 7853094]
24. Arnoczky SP, Lavagnino M, Whallon JH, Hoonjan A. In situ cell nucleus deformation in tendons under tensile load; a morphological analysis using confocal laser microscopy. J Orthop Res 2002;20:29–35. [PubMed: 11853087]
25. Merryman WD, Youn I, Lukoff HD, Krueger PM, Guilak F, Hopkins RA, Sacks MS. Correlation between heart valve interstitial cell stiffness and transvalvular pressure: implications for collagen biosynthesis. Am J Physiol Heart Circ Physiol 2006;290:H224–H231. [PubMed: 16126816]
26. Taylor PM, Batten P, Brand NJ, Thomas PS, Yacoub MH. The cardiac valve interstitial cell. International Journal of Biochemistry and Cell Biology 2003;35:113–118. [PubMed: 12479860]
27. Billiar KL, Sacks MS. A method to quantify the fiber kinematics of planar tissues under biaxial stretch. J Biomech 1997;30:753–756. [PubMed: 9239558]
28. Chaudhuri BB, Kundu P, Sarkar N. Detection and Gradation of Oriented Texture. Pattern Recogn Lett 1993;14:147–153.
29. Karlon WJ, Covell JW, McCulloch AD, Hunter JJ, Omens JH. Automated measurement of myofiber disarray in transgenic mice with ventricular expression of ras. Anat Rec 1998;252:612–625. [PubMed: 9845212]
30. Spencer, AJM. Continuum Mechanics. New York: Longman Scientific & Technical; 1980.
31. Wake MC, Gupta PK, Mikos AG. Fabrication of pliable biodegradable polymer foams to engineer soft tissues. Cell Transplant 1996;5:465–473. [PubMed: 8800514]
32. Guan J, Fujimoto KL, Sacks MS, Wagner WR. Preparation and characterization of highly porous, biodegradable polyurethane scaffolds for soft tissue applications. Biomaterials 2005;26:3961–3971. [PubMed: 15626443]
33. Guilak F, Ratcliffe A, Mow VC. Chondrocyte deformation and local tissue strain in articular cartilage: a confocal microscopy study. J Orthop Res 1995;13:410–421. [PubMed: 7602402]
34. Sarkadi B, Parker JC. Activation of ion transport pathways by changes in cell volume. Biochim Biophys Acta 1991;1071:407–427. [PubMed: 1721542]
35. Butler DL, Goldstein SA, Guilak F. Functional tissue engineering: the role of biomechanics. J Biomech Eng 2000;122:570–575. [PubMed: 11192376]
36. Merryman WD, Lukoff HD, Long RA, Engelmayr GC Jr. Hopkins RA, Sacks MS. Synergistic effects of cyclic tension and transforming growth factor-beta1 on the aortic valve myofibroblast. Cardiovasc Pathol 2007;16:268–276. [PubMed: 17868877]
37. Shelton JC, Bader DL, Lee DA. Mechanical conditioning influences the metabolic response of cell-seeded constructs. Cells Tissues Organs 2003;175:140–150. [PubMed: 14663157]
38. van der Meulen MC, Huiskes R. Why mechanobiology? A survey article. J Biomech 2002;35:404–414.
39. Isenberg BC, Williams C, Tranquillo RT. Endothelialization and flow conditioning of fibrin-based media-equivalents. Ann Biomed Eng 2006;34:971–985. [PubMed: 16783653]
40. Isenberg BC, Williams C, Tranquillo RT. Small-diameter artificial arteries engineered in vitro. Circ Res 2006;98:25–35. [PubMed: 16397155]
41. Neidert MR, Tranquillo RT. Tissue-engineered valves with commissural alignment. Tissue Eng 2006;12:891–903. [PubMed: 16674301]
42. Williams C, Johnson SL, Robinson PS, Tranquillo RT. Cell sourcing and culture conditions for fibrin-based valve constructs. Tissue Eng 2006;12:1489–1502. [PubMed: 16846346]
43. Robinson PS, Johnson SL, Evans MC, Barocas VH, Tranquillo RT. Functional Tissue-Engineered Valves from Cell-Remodeled Fibrin with Commissural Alignment of Cell-Produced Collagen. Tissue Eng. 2007
44. Freed LE, Vunjak-Novakovic G, Biron RJ, Eagles DB, Lesnoy DC, Barlow SK, Langer R. Biodegradable Polymer Scaffolds for Tissue Engineering. Bio/technology 1994;12:689–693. [PubMed: 7764913]

45. Venugopal J, Low S, Choon AT, Ramakrishna S. Interaction of cells and nanofiber scaffolds in tissue engineering. J Biomed Mater Res B Appl Biomater. 2007

46. Chen M, Patra PK, Warner SB, Bhowmick S. Role of fiber diameter in adhesion and proliferation of NIH 3T3 fibroblast on electrospun polycaprolactone scaffolds. Tissue Eng 2007;13:579–587. [PubMed: 17518604]

47. Engelmayr GC, Soletti L, Vigmostad SC, Budilarto SG, Federspiel WJ, Chandran KB, Vorp DA, Sacks MS. The flexure-stretch-flow bioreactor: A novel tool for studying heart valve tissue mechanobiology. Annals of Biomedical Engineering. in-press

48. Engelmayr GC Jr. Sacks MS. Prediction of extracellular matrix stiffness in engineered heart valve tissues based on nonwoven scaffolds. Biomech Model Mechanobiol. 2007Epub ahead of print

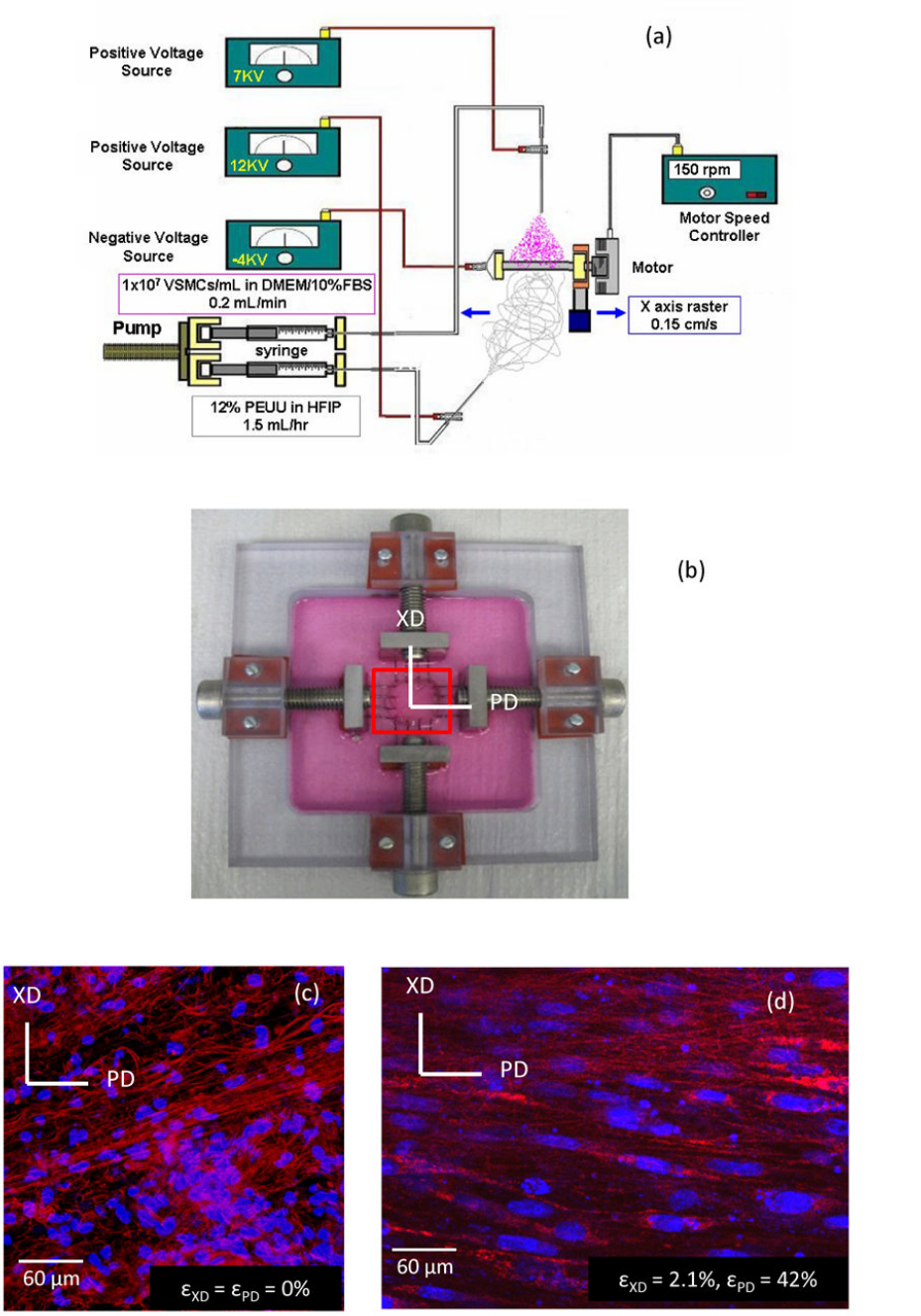

Figure 1.

Fabrication and imaging under biaxial stretch of cell integrated elastomeric scaffolds. (a) Cell-scaffold constructs were fabricated via concurrently electrospinning polymer and electrospraying cells onto a 4.7 mm diameter rotating mandrel. (b) Biaxial stretch device used to deform cell micro-integrated ES-PEUU scaffolds. (c,d) As the scaffold construct underwent strip biaxial deformation, the cell nuclei (blue) were observed to elongate and the fibers become straightened (red).

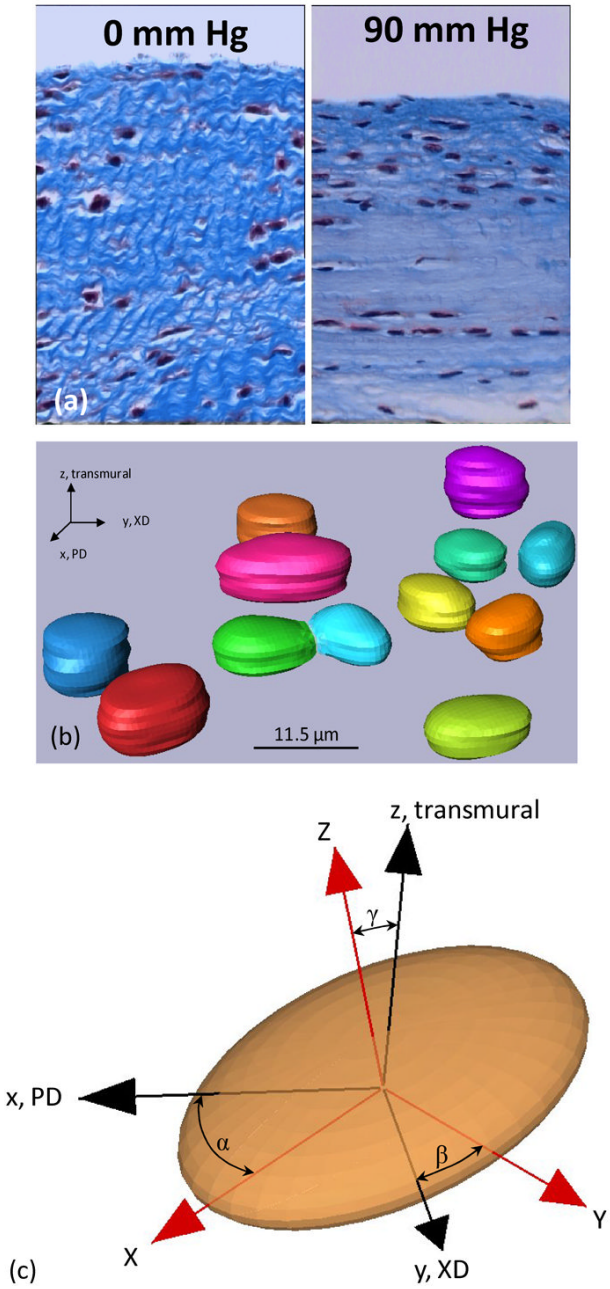

Figure 2.

Nuclear aspect ratio deformation and orientation. (a) In native tissues such as the aortic valve, cell nuclei undergo very large changes in aspect ratio induced by tissue stretch and compaction. Here aortic valve tissue cross-sections are shown in the unloaded (0 mmHg) and full physiological loaded (90 mmHg) states. (b–c) 3D reconstructions of the micro-integrated vascular smooth muscle cells in the unloaded configuration, whose 3D orientation was quantified with respect to the specimen PD and XD axes by the angles α,β, and δ.

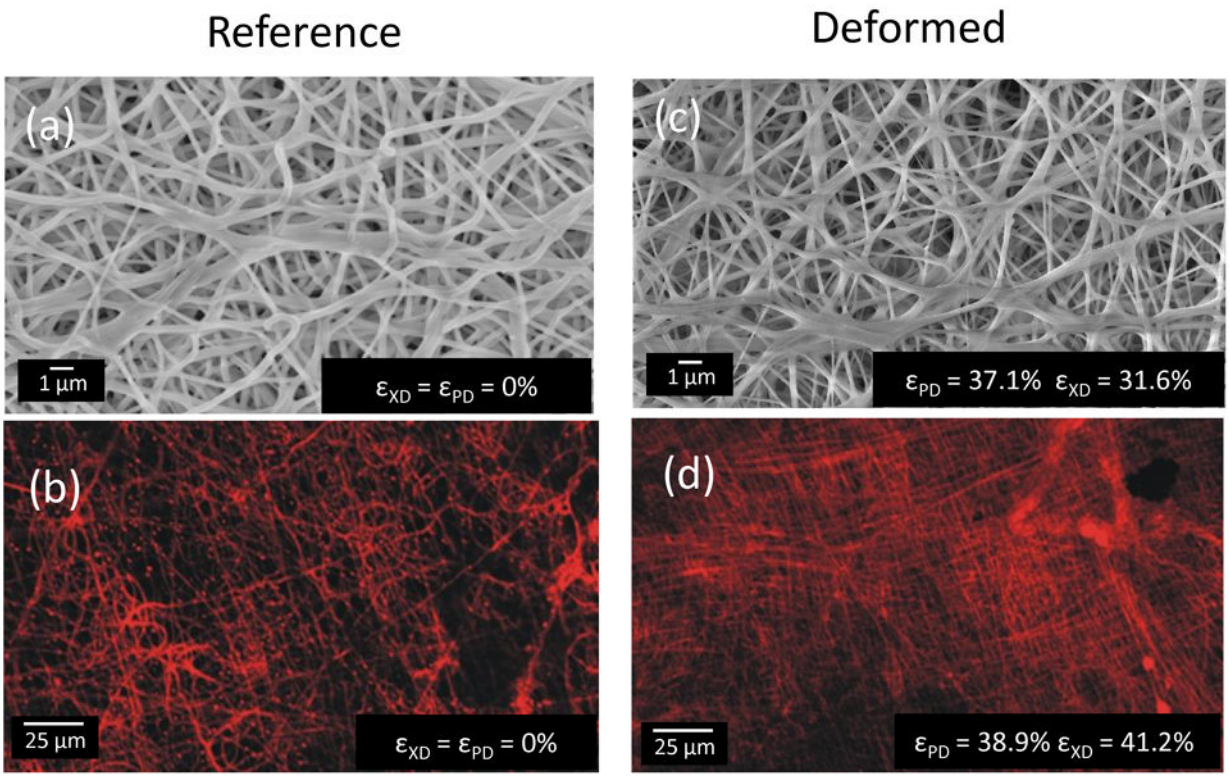

Figure 3.
Changes in ES-PEUU fiber microarchitecture under biaxial stretch. When strained equally in both orthogonal directions, PEUU fibers were observed by (a,c) SEM and (b,d) laser scanning confocal microscope to transition from a tortuous configuration in the unstrained state to an interconnected web-like architecture at high strains state.

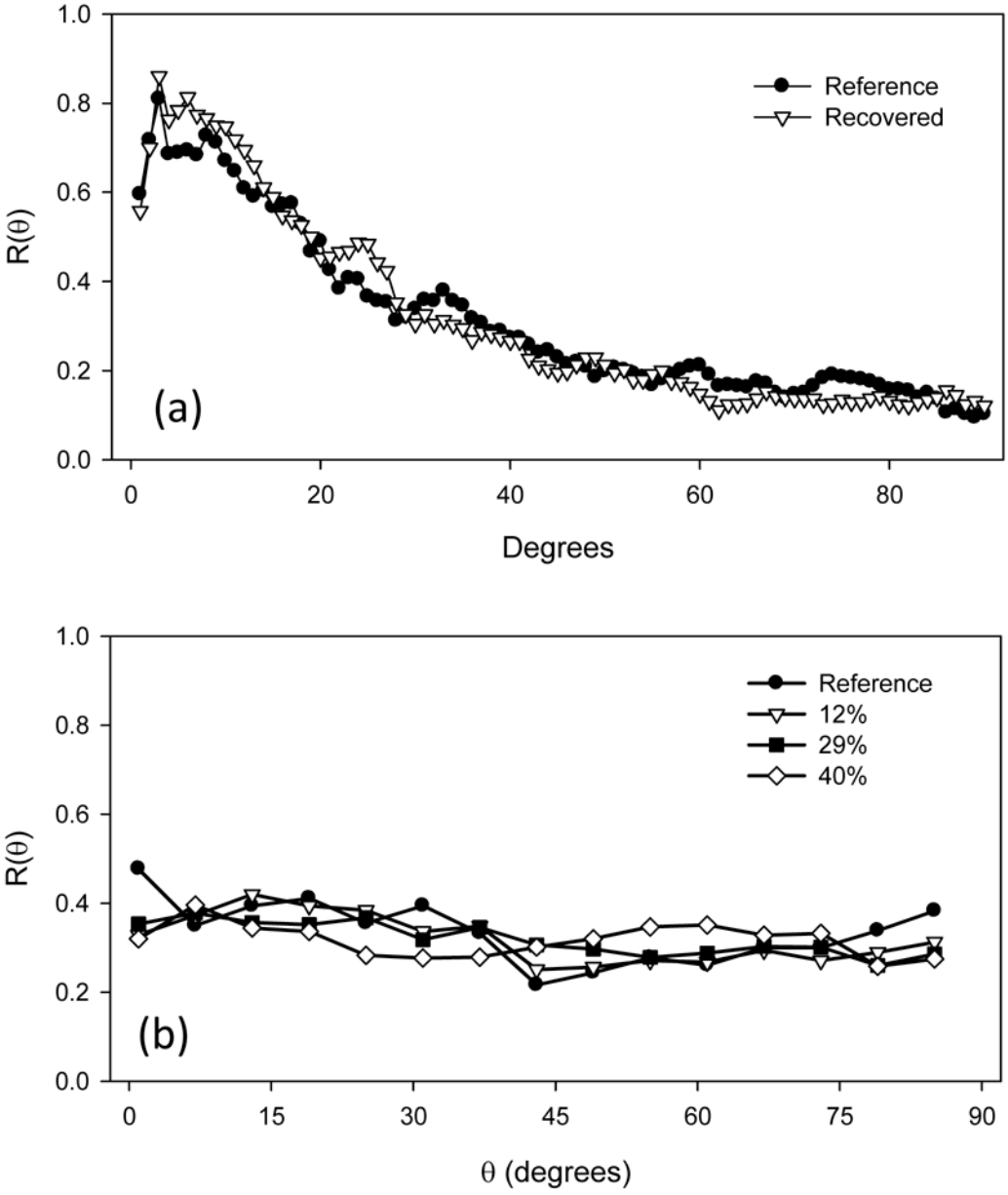

Figure 4.

(a) When strained equi-biaxially and unloaded, the ES-PEUU fibers were observed to return to their original orientations, suggesting an elastic behavior. Moreover, when strained equi-biaxially by at various levels, not detectable change in orientation occurred, as predicted by affine fiber kinematics.

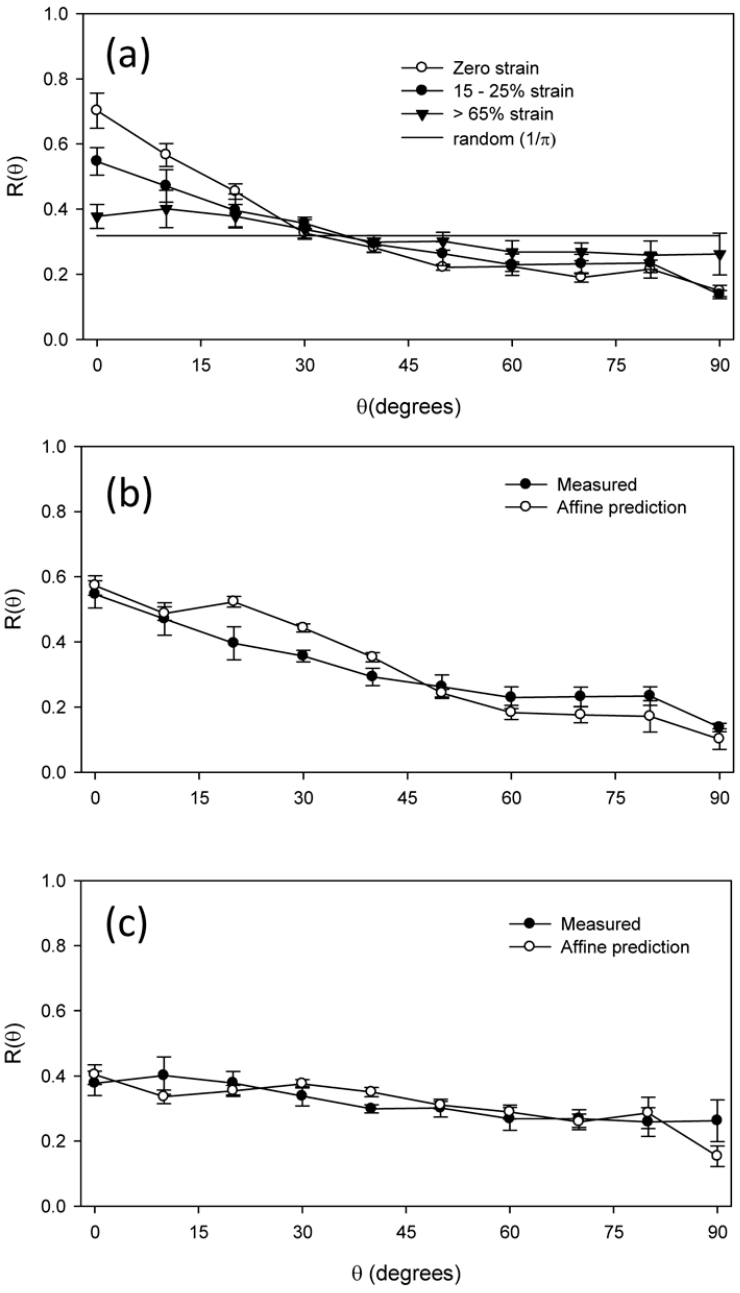

Figure 5.

ES-PEUU fiber architecture responds to strain in an affine sense. To induce the greatest fiber rotations, we strained the scaffolds along the XD direction to a mid-level (15–25%) and high (>65%), and noted a gradual shift of the fiber orientation distribution function R(θ) to a random-like distribution (where $R(\theta) = 1/\pi$) (a). When we compared the R(θ) to that predicted by an affine model (see Methods), good agreement was found at both (b) mid-level and (c) high level strains. This suggests that ES-PEUU fiber deform in a bulk sense with the macro-scaffold strains.

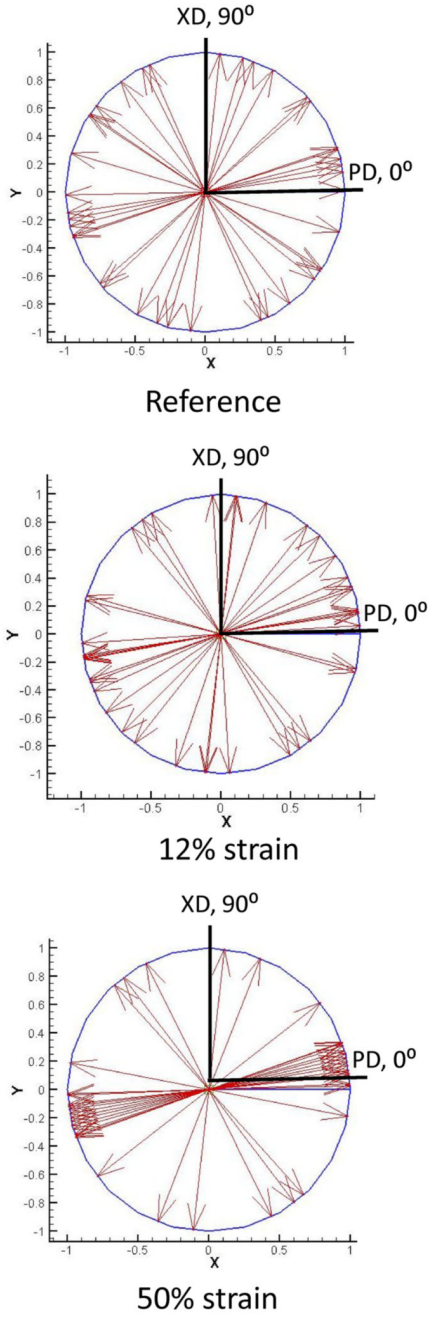

Figure 6.

Micro-integrated cell rotations during deformation. As the cell-microintegrated scaffolds were deformed under strip biaxial stretch, the integrated cells' principal component directions were observed to rotate and become more uniformly aligned in the direction of deformation. Here, this phenomenon is shown with all measured major principal directions shown as unit vectors.

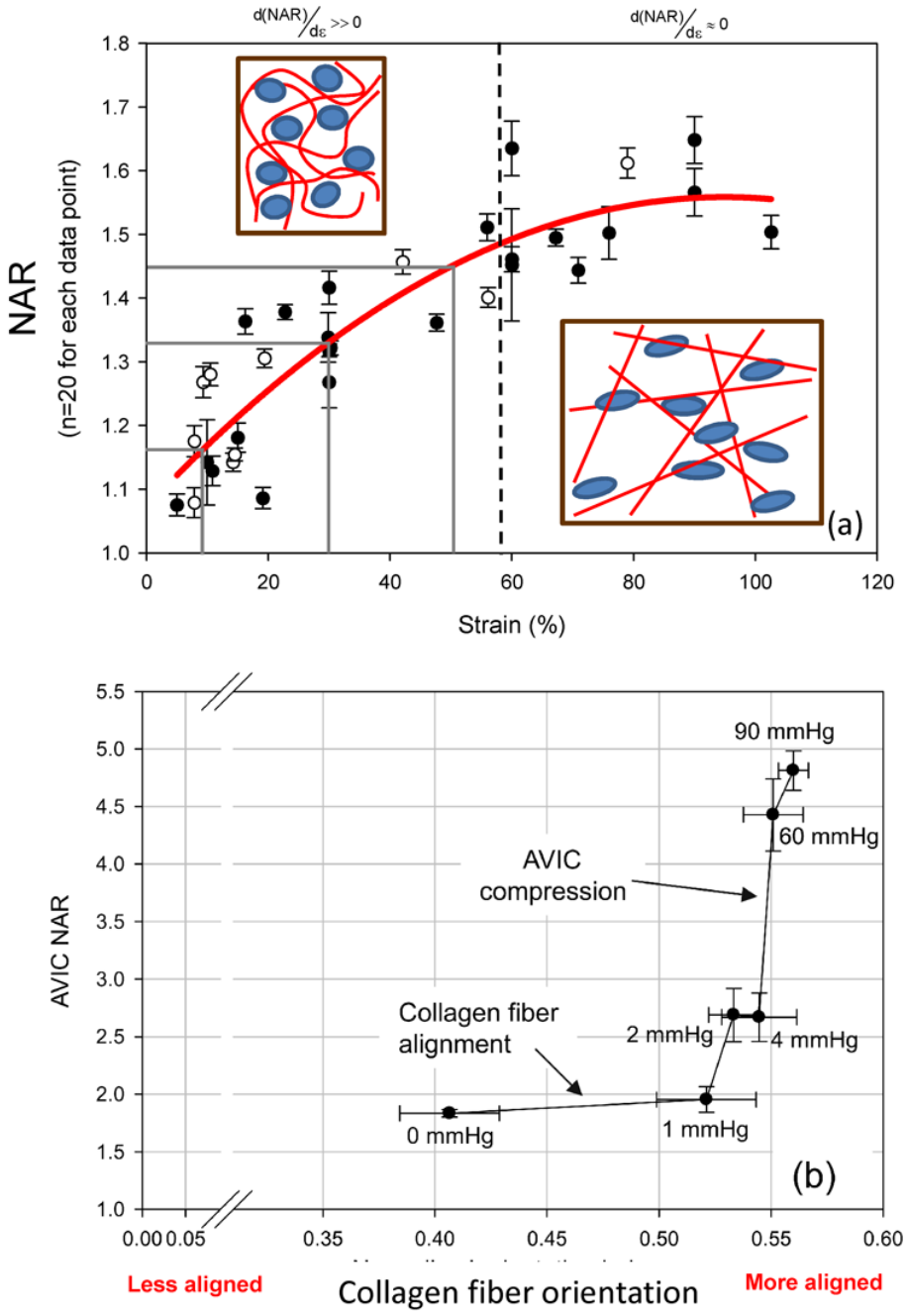

Figure 7.

NAR change with deformation is closely related to local fiber microarchitecture. (a) A composite of all NAR measurements (mean ± s.e.m) demonstrated a rapid increase to ~60% strain, after which a plateau was observed with further strain increases, indicating that nuclei deformations are dominated by local fiber straightening. (b) Cells in native tissues, in contrast, exhibit a very different response when exposed to physiologically stress levels. In this example, when compared to local collagen fiber alignment AVIC nuclear deformations undergo relatively little change at low transvalvular pressures (i.e. low tissue stresses), whereas at high transvalvular pressures (i.e. high tissue stresses) they are dominated by fiber compaction effects. Modified from [22].